Biophysical *Journal*
Article

Biophysical Society

Actin Dynamics Couples Extracellular Signals to the Mobility and Molecular Stability of Telomeres

Doorgesh Sharma Jokhun,[1] Yuqing Shang,[1] and G. V. Shivashankar[1,2,3,*]
[1]Mechanobiology Institute and [2]Department of Biological Sciences, National University of Singapore, Singapore; and [3]Institute of Molecular Oncology, Italian Foundation for Cancer Research, Milan, Italy

ABSTRACT Genome regulatory programs such as telomere functioning require extracellular signals to be transmitted from the microenvironment to the nucleus and chromatin. Although the cytoskeleton has been shown to directly transmit stresses, we show that the intrinsically dynamic nature of the actin cytoskeleton is important in relaying extracellular signals to telomeres. Interestingly, this mechanical pathway not only transmits physical stimuli but also chemical stimuli. The cytoskeletal network continuously reorganizes and applies dynamic forces on the nucleus and feeds into the regulation of telomere dynamics. We further found that distal telomeres are mechanically coupled in a length- and timescale-dependent manner and identified nesprin 2G as well as lamin A/C as being essential to regulate their translational dynamics. Finally, we demonstrated that such mechanotransduction events impinge on the binding dynamics of critical telomere binding proteins. Our results highlight an overarching physical pathway that regulates positional and molecular stability of telomeres.

INTRODUCTION

Telomeres are an important functional unit of the genome, crucial for normal cellular homeostasis (1,2). They exist at the ends of every chromosome, consist of highly conserved sequences (TTAGGG repeats in vertebrates), and are decorated by arrays of a specialized set of proteins known as the shelterin complex (3,4). These protein complexes protect genomic integrity by preventing the DNA damage-response machinery from misidentifying the ends of chromosomes as double-strand breaks (5). Defects in the binding of these proteins results in acute genomic aberrations, including chromosome end-to-end fusion (6–10). Moreover, telomere dysfunctions are hallmarks of several aging-related diseases (11–15), laminopathies (16,17), and cancers (1,8,12,18–22). Although several studies have investigated telomere stability from a biochemical point of view (23–27), the mechanical connection between the extracellular environment and telomeres is less understood. Additionally, telomeres can be used as reference points to probe chromatin dynamics in living systems. Indeed, such studies have been carried out to better understand chromatin dynamics in different cell types and under physiological as well as pathological conditions (28,29).

Besides biochemical signaling pathways, a plethora of physical links between the cell membrane and the nucleus regulate cell behavior. One key structure that physically links the extracellular microenvironment to the genome inside the nucleus is the cytoskeleton (30). This dynamic network of various filamentous proteins, adhesion molecules, adaptors, and cross-linkers has been studied in detail, particularly with respect to its response to different extracellular signals (30–37). However, the impact of intrinsically fluctuating cytoskeletal forces on the nucleus and distinct units of the genome are less explored. Specifically, it remains unclear how telomere mobility and molecular stability are regulated by extracellular-signal-induced changes in actomyosin dynamics.

Physical and biochemical stimuli such as matrix constraint (38–41), compression, and tumor necrosis factor alpha (TNF-α) stimulation (42,43) have been shown to modulate the three-dimensional organization of the nucleus and genome regulatory programs. Here, we describe the role of actomyosin force fluctuations, as regulated by these extracellular signals, on telomere (and chromatin) dynamics. We used fibronectin microcontact printing to precisely define the microenvironment at the single-cell level and subjected the cells to different extracellular cues.

We show that the intrinsic actomyosin dynamics, as observed over a seconds-to-minute timescale, was sensitive to the various perturbations. This network provides a means for the extracellular signals to be mechanically propagated to telomeres, thereby regulating their positional dynamics. We also show that telomere movements are correlated in a

Submitted March 23, 2018, and accepted for publication August 15, 2018.
*Correspondence: shiva.gvs@gmail.com
Editor: Tom Misteli.
https://doi.org/10.1016/j.bpj.2018.08.029

length-scale-dependent manner and identified lamin A/C as being the critical scaffold that anchors telomeres and governs this mechanical coupling. Finally, we demonstrate that this cytoskeleton- and nucleoskeleton-mediated mechanotransduction allows extracellular cues to modulate the turnover of essential telomere binding proteins from a distance.

MATERIAL AND METHODS

Fibronectin micropatterning

Polydimethylsiloxane (PDMS) elastomer (SYL-GARD 184; Dow Corning, Midland, MI) was prepared at a 1:10 ratio of curative/precursor according to the manufacturer's protocol. The PDMS mixture was then poured onto microfabricated silicon wafers containing an array of microwells of the desired geometry, degassed in a desiccator for 20 min, and cured for 2 h at 80°C. The solidified PDMS was subsequently peeled off the silicon mold and used as stamps to transfer fibronectin to culture dishes by microcontact printing, as explained below.

The surface of the PDMS stamps (containing protrusions with the desired geometry) was treated with high-powered oxygen plasma (Plasma Cleaner Cat. No. PDC-002; Harrick Scientific Products, Pleasantville, NY) for 4 min and fibronectin (Sigma-Aldrich, St. Louis, MO) solution (100 μg/mL) was allowed to adsorb onto the surface. The fibronectin-containing surface was then brought into contact with the culture dish (Ibidi uncoated 35 mm dishes, cat. number 81151; Martinsried, Germany), thereby depositing islands of fibronectin on the dish with the desired geometry. Once done, the PDMS stamps were carefully removed and discarded.

This resulted in an array of fibronectin islands of a defined geometry on the culture dish. The remaining area of the dish was passivated with 2 mg/mL Pluronic F-127 (Sigma-Aldrich) to ensure that the cells do not migrate out of the two-dimensional (2D) fibronectin islands. The pluronic acid treatment was carried out for 10 min, and the dish was properly washed with phosphate-buffered saline and cell culture medium before the seeding of cells.

Cell culture

Wild-type NIH 3T3 mouse embryonic fibroblasts were cultured in low-glucose Dulbecco's modified Eagle's medium (Gibco, Gaithersburg, MD; Life Technologies, Carlsbad, CA) supplemented with 10% (vol/vol) fetal bovine serum (Gibco; Life Technologies) and 1% penicillin-streptomycin (Gibco; Life Technologies) at 37°C and 5% CO_2 in a humidified incubator.

The cells were trypsinized (Gibco; Life Technologies) and seeded on the fibronectin micropatterned dishes for 10 min, after which the medium was changed to remove unadhered cells. The dishes were then kept for 3 h before imaging.

Cytochalasin D (Sigma-Aldrich) and blebbistatin (Merck, Kenilworth, NJ) were used at 500 nM and 25 μM working concentrations respectively, and cells were imaged 30 min after treatment.

All transfections were carried out using the Neon Transfection System (Thermo Fisher Scientific, Waltham, MA).

Imaging acquisition and analysis

Imaging was carried out using a 100× oil objective with a numerical aperture of 1.4 on a NikonA1R confocal microscope (Nikon, Tokyo, Japan). Time-lapse imaging of 2 min was performed at four frames per second with an open pinhole and imaging a single *Z*-slice. The pixel size was 0.05 μm. For static images, a 60× 1.4 numerical aperture oil objective was used, and the pinhole was maintained at 1 Airy unit. The pixel size was 0.2 μm in *XY* and 0.8 μm in *Z*.

Firstly, the time-lapse images were analyzed using Imaris (Bitplane, Zurich, Switzerland). A high threshold was used to track the positions of the telomeres as a function of time. Secondly, the images were analyzed using custom-written codes in MATLAB (The MathWorks, Natick, MA). A low threshold value was used so as to identify and track the entire nucleus from the diffused telomeric repeat-binding factor 1-dsRed (TRF-1-dsRed) signals. These trajectories were used both to study the nuclear translational motion and to subtract from the telomere trajectories to obtain the movement of the telomeres within the nucleus. The changes in nuclear orientation were also tracked so that angular movements coming from nuclear rotation could be subtracted from the telomere trajectories.

Fluorescence recovery after photobleaching (FRAP) was performed using a 40× air objective. The pinhole was kept open, and images were acquired every 1.5 s for 3 min. A circular region of interest of 0.8 μm in diameter was used to bleach the telomeres, and three images were acquired as reference before bleaching. Imaris (Bitplane) was used to track the bleached telomeres and measure their intensity at each time point. The normalized intensity (I_{norm}) was then calculated according to the following formula:

$$I_{norm}(t) = \frac{I(t) - I_B(t)}{<I_{pre-bleach} - I_B>} \times \frac{<T_{pre-bleach} - I_B>}{T(t) - I_B(t)},$$

where $I(t)$ is the measured intensity in the bleached area, $I_B(t)$ is the background intensity, $<I_{pre\text{-}bleach} - I_B>$ is the average background-subtracted intensity before photobleaching in the bleached region, $<T_{pre\text{-}bleach} - I_B>$ is the average intensity of the whole nucleus before bleaching, and $T(t)$ is the intensity of the whole nucleus. The first factor in the equation allows us to calculate the recovery fraction, normalizing $I(t)$ to the initial value and rescaling it between 0 and 1. The second factor compensates for the overall bleaching of the nucleus by normalizing the intensity in the bleached area to the total intensity of the nucleus.

Subsequently, the normalized recovery curves were fitted with an exponential function of the form $I = A(1 - e^{-kt})$. The values of A and k were used as the mobile fractions and the inverse recovery rates of TRF-1 for every bleached telomere.

Quantifying actin alignment

Immunofluorescent images of phalloidin-stained cells were segmented into squares of 2 μm (100 pixels). For each square, every pixel was mapped onto a Cartesian plane with the pixel value treated as the number of points at that location on the Cartesian plane. Subsequently, a principle component analysis was performed, and the orientation of the principle component was used as the local orientation of actin for each 2-μm square. Finally, the mean orientation was calculated, and all the local orientations were recalculated relative to the mean direction.

RESULTS

Extracellular signals alter nuclear dynamics by modulating cytoskeletal forces

We used fibronectin microcontact printing as a tool to homogenize the physical boundary condition of NIH 3T3 fibroblasts at the single-cell level. This allowed us to precisely control the cues the cells experience from the extracellular environment (Fig. 1 *a*). The cells were transfected with TRF-1-dsRed (telomeric repeat-binding factor 1), which is a component of the shelterin complex, before their seeding on the micropatterned substrate. Because TRF-1 is localized only in the nucleus, it can be used to track

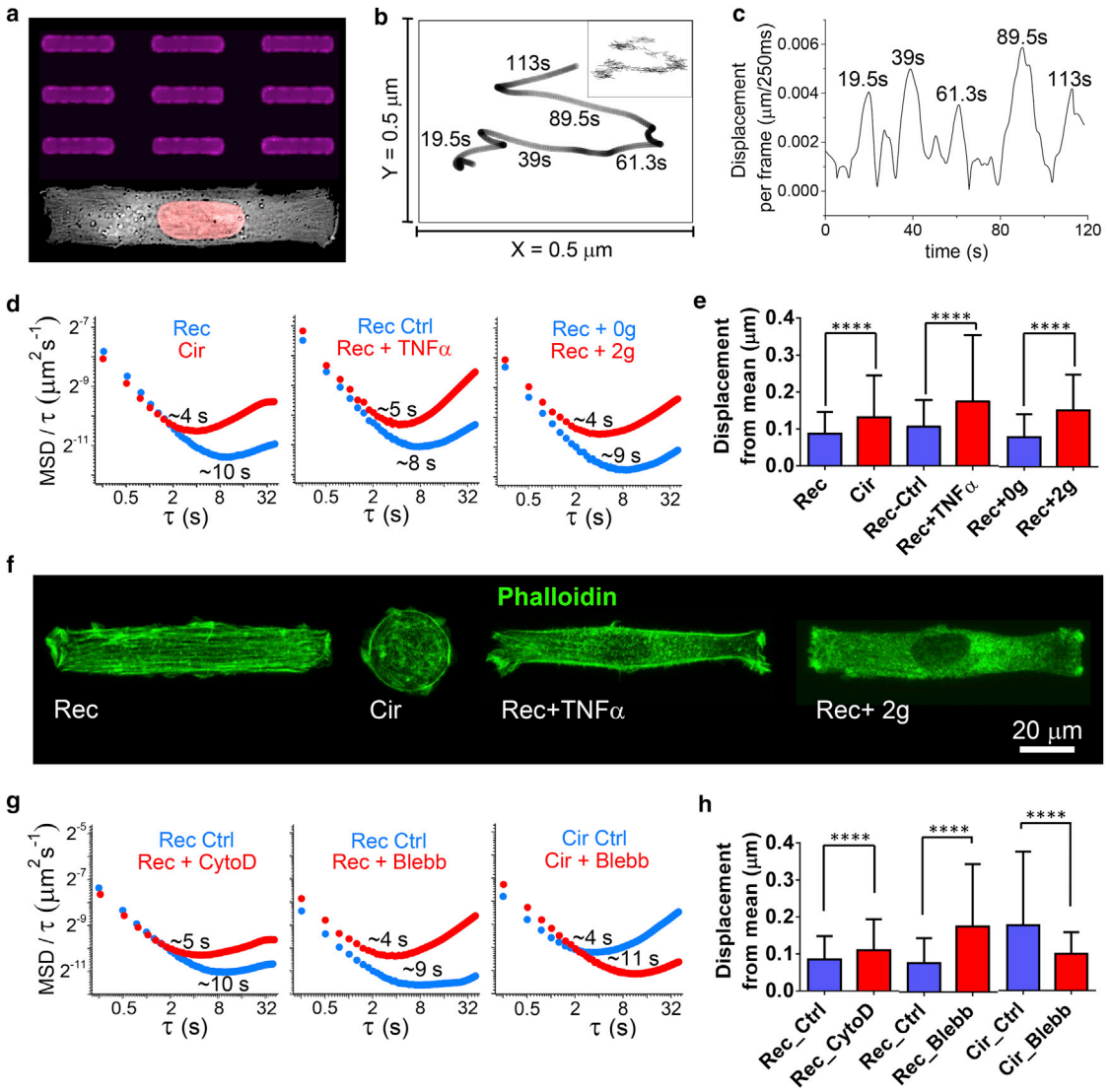

FIGURE 1 Extracellular physicochemical signals are mechanically relayed to the nucleus via actomyosin remodeling dynamics. (*a*) An array of microcontact-printed fibronectin islands on a culture dish visualized using Alexa Fluor 647 dye (*top*). A typical cell seeded on the rectangular pattern (*bottom*). The gray signal is from the transmitted light, and the red signal is from diffused TRF-1-dsRed inside the nucleus. (*b*) The nuclear trajectory of a cell seeded on the rectangular pattern imaged at 4 frame/s (*inset*). The robust lowess-smoothed trajectory of the nucleus with a window of 10 s . (*c*) Instantaneous speed of the nucleus extracted from the smoothed trajectory as a function of time. (*d*) Plots of average $\langle r^2(\tau)\rangle/\tau$ as a function of τ for nuclei of cells under the mentioned conditions. (*e*) The mean of the displacement of nuclei from their mean positions within time windows of 2 min. (*f*) Phalloidin staining showing the actin organization in cell under the mentioned conditions. (*g*) Plots of average $\langle r^2(\tau)\rangle/\tau$ as a function of τ for nuclei of cells treated with the mentioned cytoskeletal targeting drugs. (*h*) The mean of the displacement of nuclei from their mean positions within time windows of 2 min. Error bars represent SD. A Kolmogorov-Smirnov test was carried out to determine statistical significance.

movements of both the entire nucleus, as well as individual telomeres, by applying a low or high threshold respectively, during postimaging analysis.

With a temporal resolution of 250 ms and total imaging time of 2 min, we observed that the nucleus continuously alternated between immobile and mobile phases, even without external disturbances. The raw nuclear trajectory (*inset*) was smoothed using a robust lowess filter with a span of 10 s to remove high-frequency fluctuations and reveal the overall trend of the motion (Fig. 1 *b*). The shifts between the two phases of motion are clearly seen from the oscillating speed-time graph of the smoothed nuclear trajectory (Fig. 1 *c*).

To quantitatively describe the movement of the nucleus as well as its interaction with its surroundings, the time-averaged mean-squared displacement (MSD) of its centroid was calculated for timescales (τ) ranging from 250 ms to 40 s. For normal diffusion, the MSD is given by $<r^2(\tau)> = 2dD\tau$, where $r(\tau)$ is the vector displacement of the centroid within all possible time windows of size τ, d is the number of spatial dimensions (= 2), and D is the diffusion coefficient. When the random motion of the particle

is constrained or guided by its surrounding, it results in anomalous diffusion, which is given by $<r^2(\tau)> = D_\alpha \tau^\alpha$. When the exponent α is less than 1, the motion is said to be subdiffusive, and when it is greater than 1, the motion is said to be superdiffusive. Note that when $\alpha = 1$ (normal diffusion), the MSD varies linearly with τ and $D_\alpha = 2dD$. A convenient way of analyzing the diffusive property of the particle as a function of timescale is to plot MSD/τ as a function of τ on a log-log scale $[\log(r^2(\tau)/\tau) = (\alpha - 1)\log\tau + \log D\alpha]$ (44,45). In such a situation, subdiffusion appears with a negative slope (gradient, $\alpha - 1 < 0$), normal diffusion appears as a horizontal line ($\alpha - 1 = 0$), and superdiffusion appears with a positive slope ($\alpha - 1 > 0$). Additionally, during normal diffusion, the Y value of the horizontal line is proportional to the diffusion coefficient ($= 2dD$).

The MSD/τ plot showed two distinct regimes for the nuclear motion (Fig. 1 *d*). At small timescales, the nucleus moves in a constrained diffusive manner, whereas at larger timescales, it moves with a superdiffusive behavior. For the unperturbed cells on rectangular patterns, the transition between these two regimes occurred at a timescale of around 10 s and the corresponding diffusion coefficient was on the order of 10^{-4} μm^2 s^{-1}.

To assess the effects of extracellular signals on the dynamics of intracellular force fluctuations, we plotted the MSD/τ vs. τ of the nuclear motion with three different kinds of perturbations: 1) a physical constraint by seeding the cells on small circular patterns of 500 μm^2, 2) a biochemical signal by stimulating the cells with TNF-α, and 3) a compressive force by applying a load of $\sim 10^{-6}$ N per cell. For each extracellular change, we observed a decrease in the transition timescale as well as an increase in the diffusion coefficient (Table S1). We also observed an increase in the average displacement of the nuclei from their mean positions within the observational window of 2 min (Fig. 1 *e*).

The actin cytoskeleton is known to regulate nuclear position and positional dynamics (39,46,47). For this reason, we investigated whether different extracellular cues were impinging on nuclear dynamics by modulating the actin cytoskeleton. Phalloidin staining showed that the structural organization of actin filaments was different under the four conditions (Fig. 1 *f*). Although F-actin was present as long apical stress fibers in unperturbed cells on rectangular patterns, it appeared fragmented and punctated when the extracellular condition was changed. To further confirm that the nuclear dynamics was altered by changes in the actomyosin network, we directly treated cells seeded on the rectangular patterns with the actin-depolymerizing drug cytochalasin D, as well as the myosin II inhibitor blebbistatin. In both cases, we successfully recapitulated the kind of nuclear dynamics we had observed by altering the extracellular cues (Fig. 1, *g* and *h*). Interestingly, on the circular geometry, blebbistatin treatment resulted in increased transition timescale and decreased diffusion coefficient (Fig. 1, *f* and *g*). This means that although actomyosin tension stabilizes the nuclear position in the presence of apical stress fibers, myosin activity also drives nuclear translational dynamics when actin filaments are in the form of smaller fragments. This is in line with our previous study on the role of cell geometry on nuclear deformability (38).

We then decomposed the nuclear movement of the unperturbed rectangular cells along the major and minor axes and observed that there was an anisotropy in the 2-min nuclear trajectories. The nucleus traveled more along the major axis of the cell (defined as the X direction) compared to the perpendicular direction (Fig. S2 *a*). Given the short timescale of 2 min and the diffusion length scale of less than 0.5 μm, it is improbable that the anisotropy is a result of the nucleus being restricted by the cell membrane. To confirm this, we fixed a large population of cells and measured the displacements of their nuclei relative to the center of each cell. These measurements served as a proxy to estimate the nuclear displacement typically allowed by the cells (Fig. S2 *b*). Indeed, we found that during the 2-min live experiments, the nuclei explored only a tiny fraction of the allowable displacements along both the X and Y axes. We then investigated the differential diffusive behavior of the nucleus along the two axes (Fig. S2 *c*) and observed two distinct diffusive responses. Specifically, a higher diffusion coefficient and a smaller transition timescale characterized nuclear motion along the X axis of the cell.

Because actin stress fibers are physically coupled to the nucleus via LINC complexes (48–52), we hypothesized that it is the ordered and aligned actin organization (Fig. 1 *f*) in the unperturbed rectangular condition that causes this differential movement of the nucleus. In agreement with this, the extracellular perturbations that had earlier affected actin organization also resulted in a decrease in the anisotropic movement of the nucleus along the X and Y axes (Fig. S2, *d–f*). The change, relative to the unperturbed rectangular condition, was observed both in terms of the diffusion coefficient and the transition timescale and was more pronounced along the Y axis.

As nuclear movement was found to be isotropic in cells confined to circular substrates, we quantified the alignment of actin filaments, which was assessed based on the intensity of phalloidin staining, in the rectangular and circular conditions (Fig. S2 *g*). The narrow histogram peak obtained from the rectangular condition clearly shows that the actin filaments are strongly aligned in a single direction in each cell. On the other hand, the absence of such a peak in the circular condition reflects the fact that there is no preferential alignment of actin along any axis. Finally, we analyzed the movement along the XY axis of nuclei in cytochalasin-D-treated rectangular cells. Indeed, depolymerizing F-actin ectopically caused the nucleus to move

in a more isotropic manner even in the rectangular condition (Fig. S2 *h*).

Telomere dynamics is regulated by active cytoskeletal forces

With the aim of probing how altered cytoskeletal forces impinge on genome regulation, we decided to study the spatiotemporal dynamics of telomeres. To do this, we analyzed nuclei images using a high threshold and employing single-particle-tracking algorithms to track the position of individual telomeres as a function of time (Fig. 2 *a*). Because the telomeres are within nuclei that are not stationary, we first had to account for drift in the telomere trajectories. For this, a custom MATLAB code was written to analyze images using a low threshold and determine the translational and rotational movement of the entire nucleus in each frame. We then subtracted the nuclear translational and rotational movement from the raw telomere trajectories (Fig. S3 *a*). The corrected trajectories were subsequently used for further analyses.

The corrected telomere trajectories were superimposed onto each other to quantify the space that telomeres explore within the time window of 2 min. As seen from the insets of Fig. 2 *b*, telomeres of cells under the circular condition tended to explore a larger area compared to those of cells in the rectangular condition. In the unperturbed rectangular cells, we observed a narrow probability distribution function with a high peak at the mean position, whereas the opposite was observed in the cells under the circular condition (Fig. 2 *b*). The SD of this distribution was used as a measure of the radius of constraint (R_c) of the telomeres and was calculated for the different conditions. Contour plots of the probability distribution function of the telomeres from cells in both rectangular and circular conditions are shown in Fig. S3 *b*. Although a change in cell shape resulted in the largest increase in R_c, TNF-α and compressive load also caused telomeres to explore larger areas (Fig. 2 *c*). Drug treatments revealed that myosin activity not only plays a role in anchoring telomeres in the presence of apical actin stress fibers but also in jiggling telomeres when F-actin is in a more fragmented form (Fig. 2 *d*). If telomere motion is brought about by fluctuations happening outside the nucleus, it is expected that the former is correlated with nuclear envelope fluctuations. Indeed, the motion of telomeres was found to be positively correlated to fluctuations of the nuclear envelope (Fig. S4, *c* and *d*). The correlation was stronger for telomeres nearer to the envelope.

To appreciate the timescale-dependent telomere diffusion, their MSD/τ was plotted as a function of τ on a log-log scale. The comparison between cells seeded on the rectangular patterns and those on small circular patterns is shown in Fig. 2 *e*. In both cases, we found that the telomeres undergo subdiffusive behaviors. Although the gradient became less negative with increasing timescale, it did not reach zero within a timescale that we could analyze accurately. Experiments performed by Bronshtein et al. showed that this holds true even at larger timescales

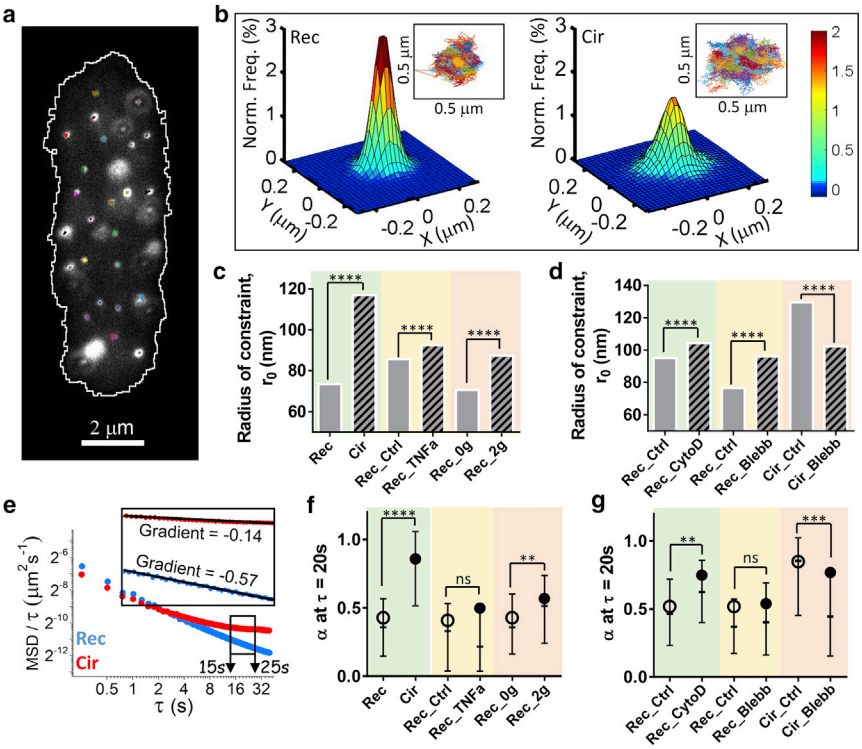

FIGURE 2 Actomyosin forces regulate the translational dynamics of telomeres. (*a*) Superimposition of TRF-1-dsRed florescent image with the detected nuclear edge as well as the trajectories of individual telomeres over a time window of 2 min. (*b*) 2D histograms showing the probability distribution function of all the telomeres from their mean positions in a time window of 2 min. The insets show the overlay of all the telomere trajectories from cells seeded on the rectangular and circular patterns, respectively. (*c* and *d*) SD of the probability distribution function of telomeres under the mentioned conditions. Statistical significance was calculated using the F-test of equality of variances. (*e*) Average $\langle r^2(\tau)\rangle/\tau$ as a function of τ for telomeres from cells seeded on the rectangular and circular patterns. The inset shows a zoomed-in view for the interval $15 < \tau < 25$ with linear fits to the data. (*f* and *g*) $<\alpha>$ exponent of the telomeres extracted from the individual MSD graphs in the interval $15 < \tau < 25$. The bars represent the 25th, 50th, and 75th percentiles. A Kolmogorov-Smirnov test was carried out to determine statistical significance.

(53). To compare different conditions, we decided to fix an arbitrary timescale of 20 s and extract the gradient of the tangent at that point. As seen in Fig. S3 *c*, the choice of 20 s as reference did not influence the results because the α-value of the rectangular condition is about half that of the circular condition across all timescales. A summary of α-values at 20 s for the various extracellular conditions is shown in Fig. 2 *f*. A mean α of 0.43 shows that telomere motion is very constrained in the unperturbed rectangular condition. In the small circular condition, on the other hand, a mean α of 0.86 shows that telomere motion approaches free diffusion. No significant change was observed upon TNF-α stimulation, and only a slight increase was observed upon application of the compressive force (Fig. 2 *f*). Although the depolymerization of apical actin stress fibers did cause an increase in the value of α in the large rectangular condition, myosin inhibition did not have a significant effect (Fig. 2 *g*). In the small circular condition, myosin inhibition resulted in a decrease in the value of α, suggesting that myosin activity exerts random forces on the telomeres.

Positional dynamics of telomeres is spatially and temporally correlated

After looking at how individual telomeres explore the space around them, we zoomed out and studied their collective movements. Toward this, we calculated the correlation between the corrected trajectories of every possible pair of telomeres from each nucleus. The result from a typical cell seeded on the large rectangular substrate is shown as a correlation matrix in Fig. S4 *a*. A corresponding matrix of *p*-values was constructed to test the null hypothesis and identify the pairs with correlation values significantly more or significantly less than zero (Fig. S4 *a*). Interestingly, we found that irrespective of cell shape, more than 60% of the possible telomere pairs were significantly positively correlated (correlation greater than 0 and $***p < 0.001$) (Fig. 4 *b*). If the telomeres moved independently, the majority of telomere pairs would be expected to be uncorrelated, and there would have been two smaller fractions with significant positive and significant negative correlation by random chance.

To further investigate this coupling between distal telomeres, we built a matrix of separation of every telomere with respect to every other telomere in each nucleus as a function of time. A schematic of this analysis is shown in Fig. 3 *a*, and a video of how the matrix evolves with time can be found in Video S1. We then linearized the matrix into a 2D kymograph in which each column corresponds to one telomere pair, the vertical axis represents time, and the color gradient represents changes in separation (Fig. 3 *b*). We observed that within any given nucleus, all telomere pairs do not go further apart or come closer together. This means that within the timescale of the experiment, we did not observe any contraction or expansion of the nucleus itself.

The SD in separation between a pair of telomeres over the period of 2 min can be used as a measure of mechanical coupling between them; the lower the SD, the more coupled those telomeres are. Our analysis revealed that cells confined to small circular substrates and those experiencing the compressive load showed reduced mechanical coupling between the telomeres (Fig. 3 *c*). This means that the telomeres were moving more freely and independently. TNF-α, on the other hand, did not have a significant effect (Fig. 3 *c*). Although the telomeres may be coupled to each other by internal cross-linking within the nucleus or via the lamina, there is also the possibility that they are linked via the cytoskeleton from outside the nucleus. Indeed, weakening the apical stress fibers in cells on the rectangular substrates, either by cytochalasin D or blebbistatin, resulted in reduced mechanical coupling between the telomeres (Fig. 3 *d*). Under the small circular condition, however, in which actomyosin fragments apply uncorrelated forces all around the nucleus, blebbistatin treatment resulted in an increase in correlation between the telomeres (Fig. 3 *d*).

Digging further, we explored how the mechanical coupling between telomeres is related to their separation and sought to determine the factors that contribute to this relationship. To this end, we plotted the SD in separation as a function of separation for all possible pairs of telomeres in each nucleus. The results shown in Fig. S4, *c* and *d*, which are from a cell seeded on the large rectangular substrate and one seeded on the small circular substrate, reveal a clear inverse relationship between mechanical coupling and telomere separation. The gradient of this relationship was used as a measure of the decay in mechanical coupling as a function of separation. Analysis of all nuclei showed that the rate of decay in mechanical coupling with separation of telomeres was higher in cells confined to small circular substrates (Fig. 3 *e*). This means that in the nuclei of cells under this geometric constraint, the system is more fluidic, and as soon as two telomeres are slightly further apart, their correlation is lost. In the nuclei of cells confined to rectangular substrates, on the other hand, the system is more rigid and even distant telomeres are elastically coupled. TNF-α and compressive load did not affect the rate of decrease in correlation as a function of length scale (Fig. 3 *e*). Interestingly, when cells were confined to rectangular substrates, cytochalasin D and blebbistatin had no effect (Fig. 3 *f*). Together with the previous result, this suggests that although the actomyosin network contributes to the positive correlation between telomeres, it does not influence the length scale over which telomeres experience an elastic coupling. This could therefore be an intrinsic property of the nucleus. Blebbistatin treatment of cells confined to the small circular substrate, however, increased the length scale over which the telomeres appear to be coupled (Fig. 3 *f*). One possible explanation for this is that under this geometric

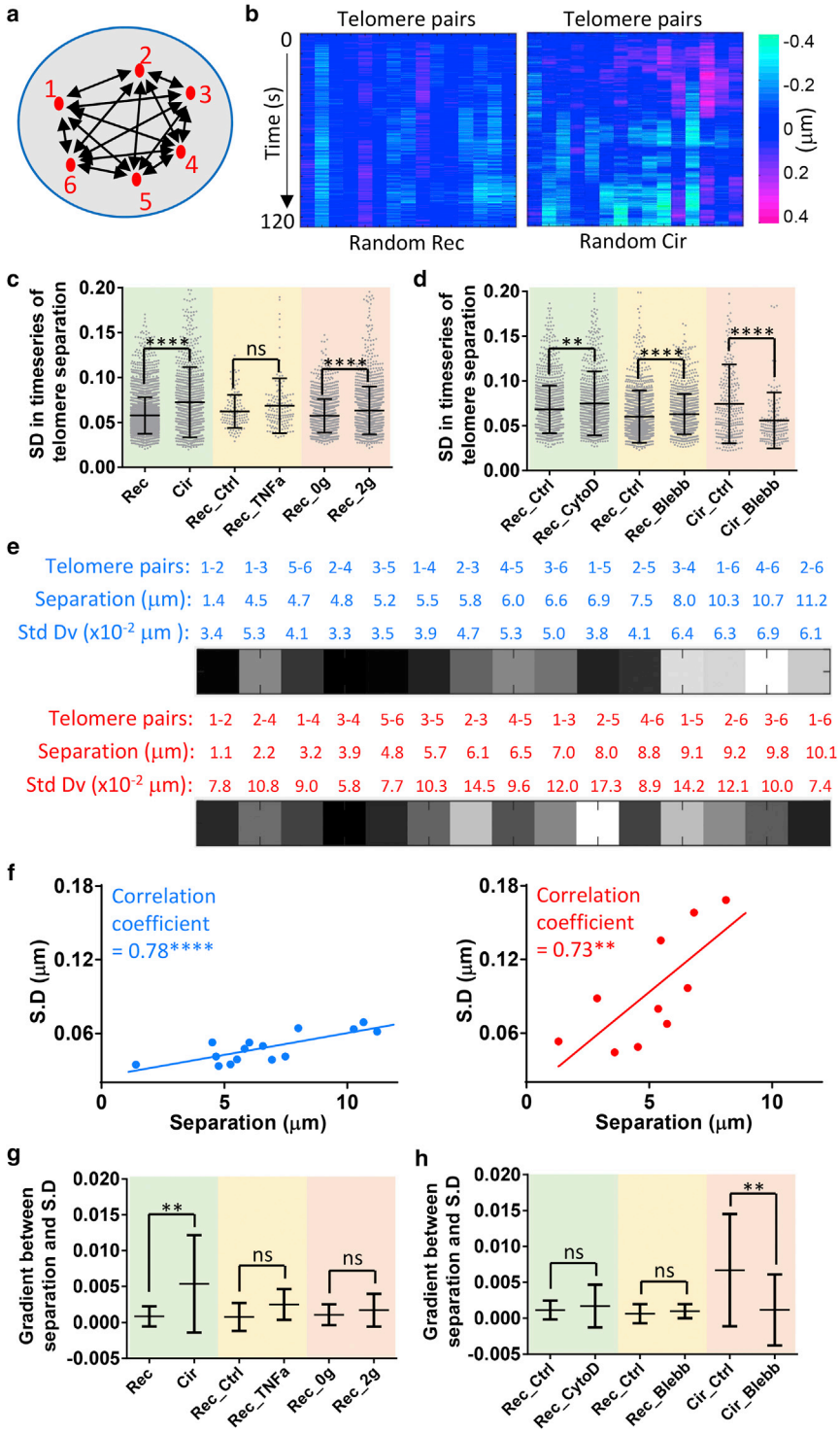

FIGURE 3 Telomeres are mechanically coupled in a length-scale-dependent manner. (*a*) A schematic of intertelomeric separations. Each red dot represents a telomere. (*b*) A kymograph of changes in separation between telomere pairs as a function of time. (*c* and *d*) SD in the separation between telomere pairs over a time window of 2 min. The dots represent individual data points, and the bars represent the mean and SD of the distribution. (*e*) A heat map showing a general increase in the SD in separation within telomere pairs with increasing separation between the telomeres. (*f*) Linear fits between the SD in separation within telomere pairs and separation between the telomeres for a typical rectangular and a typical circular cell. (*g* and *h*) The relationship between separation between telomeres and the SD in their separation. The central bar represents the mean, and the extremities the SD. A Kolmogorov-Smirnov test was carried out to determine statistical significance.

confinement, there is reduced elasticity, which would allow uncorrelated myosin-dependent forces from outside to displace individual telomeres without efficient force transmission to other telomeres.

Given the mechanical coupling of telomeres was dependent on their separation, we next investigated the timescale over which this coupling occurred. For this, from each nucleus, we selected the telomere pairs that had a significantly positive correlation. We then segmented their trajectories into all possible fragments with durations ranging from 2 to 110 s. Using these fragments, we computed the cosine of the angle between the direction vectors of each of the selected telomere pairs at timescales ranging from 2 to 110 s. For each telomere pair, the time-averaged cosine

was then plotted as a function of timescale (Fig. S5, *a* and *b*). In this analysis, an average cosine value of 1 indicates that on average, the two telomeres in question moved in the same direction over the corresponding timescale, whereas a value of −1 indicates that they moved in opposing directions and a value of 0 indicates that they moved perpendicular to each other. Our results show a progressive increase in the average cosine value with timescale, suggesting that, for correlated telomere pairs, their movements occurring over short durations are less synchronized compared to their movements over longer timescales.

Interestingly, however, in cells confined to rectangular substrates, numerous telomere pairs start to decouple and move in opposite directions when the timescale exceeds 60 s (Fig. S5 *a*). The same is observed in cells confined to small circular substrates when the timescale exceeds 80 s (Fig. S5 *b*). This suggests that one of the telomeres in the pair recoils after being displaced to its maximum. Alternatively, this may represent the timescales at which components keeping the telomeres connected begin to turn over. Fig. S5 *c* shows a summary of the timescale dependence of the mechanical coupling between significantly positively correlated telomere pairs under the different extracellular perturbations.

Cytoskeleton-mediated telomere dynamics is modulated by both the LINC complex and lamin A/C levels

From the previous results, it is clear that the cytoplasmic actomyosin network does not act alone in mediating the regulation of telomere coupling and dynamics by extracellular cues. Because altered cell shape has been shown to affect cytoskeletal connections to the nucleus and vice versa (41,54), we decided to examine the role played by some of the major components at the interface between actin and chromatin on telomere mobility.

A meshwork of type V intermediate filaments, the lamina, is found underneath the inner nuclear membrane (55) and provides structural integrity to the nucleus (56). Previous work from our lab has shown that seeding NIH 3T3 fibroblasts on small circular patterns leads to a transcriptional downregulation of lamin A/C (38), the component of the lamina that contributes to nuclear stiffness (57,58). Crossing the inner and outer nuclear membrane is the LINC complex, which physically connects chromatin to cytoskeletal structures. The complex is composed of Sad1-UNC84-domain proteins, which bind to chromatin (directly or via adaptors) and span the inner nuclear membrane, and Klarsicht/ANC-1/Syne homology (KASH)-domain proteins, which span the outer nuclear membrane and bind to various cytoskeletal filaments outside the nucleus (48,49,51,52,55).

To investigate the importance of the abovementioned components in enabling the proper regulation of telomere dynamics and docking by the cytoskeleton, before seeding the cells on the rectangular and circular patterns, they were cotransfected with either *TRF-1*-dsRed + dominant negative (DN)-KASH-enhanced green fluorescent protein or *TRF-1*-dsRed + *LMNA*-enhanced green fluorescent protein, respectively. DN-KASH is a dominant negative form of nesprin 2G, the KASH-domain protein that specifically links Sad1-UNC84-domain proteins to actin filaments (59). *LMNA* is the gene that translates to lamin A/C, and it was overexpressed to oppose the transcriptional downregulation of lamin A/C, which usually occurs when the cells are seeded on the small circular patterns (38). Additionally, we imaged $LMNA^{-/-}$ mouse embryonic fibroblasts (60) on the large rectangular patterns. The nuclear translational dynamics observed under these conditions is given in Fig. S6, *a–d* and Table S2.

Disruption of nesprin 2G caused an increase in the radius of constraint of the telomeres but a slight decrease in the α exponent of the MSD (Fig. 4, *a* and *b*). This means that although its connection to actin fibers restricts the amplitude of telomere movement, it also provides a means for fluctuating forces from outside the nucleus to displace telomeres in a more diffusive manner within the increased confinement. Surprisingly, no significant change was observed in the correlation between telomere trajectories (Fig. 4 *c*). This suggests that it is the internal components of the nuclear matrix that mechanically couple telomeres together. Consistent with this, the rate of decay in correlation as a function of separation was also unaltered in the DN-KASH transfected cells (Fig. 4 *d*).

Lamin A/C plays a predominant role in telomere tethering and dynamics. We observed a large increase in the radius of constraint as well as in the α exponent of the MSD of the telomeres when the $LMNA^{-/-}$ cells were seeded on the large rectangular patterns (Fig. 5, *a* and *b*). The telomeres seemed completely unconstrained, with an average α-value of around 1 (apparent free diffusion). In line with the deduction that the telomeres were free to move, we observed a dramatic increase in the SD of the separation between the various telomere pairs over time (Fig. 4 *c*), indicating that the telomeres moved independently from each other. We also noted an increase in the rate at which correlation between telomeres decay as a function of their separation (Fig. 4 *d*). This indicates that the nuclear environment becomes very viscous upon lamin A/C knockout.

To further decipher the role of lamin A/C in regulating telomere coupling and dynamics, we performed the reverse experiment with lamin A/C overexpression on the small circular pattern. Surprisingly, we observed an increase in the radius of constraint of the telomeres upon overexpression of lamin A/C, whereas the α-value remained in free diffusive territory (Fig. 4, *a* and *b*). These results were counterintuitive because in the large rectangular condition, the same trends were observed upon knockout of lamin A/C. It appears that increased lamin A makes the nuclear membrane more elastic and efficient at transmitting cytoskeletal

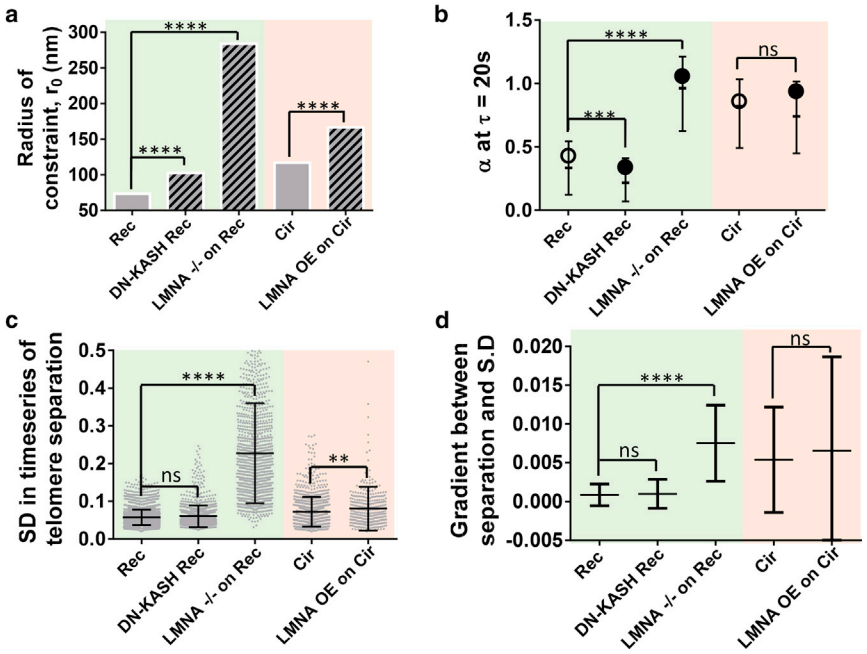

FIGURE 4 Cytoskeleton-mediated telomere dynamics and coupling rely on functional LINC complexes and stability of lamin A/C in the nuclear lamina. (*a*) The SD of the probability distribution function of telomeres under the mentioned conditions. Statistical significance was calculated using the F-test of equality of variances. (*b*) The $<\alpha>$ exponent of the telomeres extracted from the individual MSD graphs in the interval $15 < \tau < 25$. The bars represent the 25th, 50th, and 75th percentiles. (*c*) The SD in the separation between telomere pairs over a time window of 2 min. The dots represent individual data points, and the bars represent the mean and SD of the distribution. (*d*) The relationship between separation between telomeres and the SD in their separation. The central bar represents the mean, and the extremities the SD. A Kolmogorov-Smirnov test was carried out to determine statistical significance.

fluctuations. Although in the wild-type condition, the forces are attenuated during deformation of the nuclear membrane (viscous), in the *LMNA* overexpression system, the membrane is highly elastic and dynamic cytoskeletal forces are more efficiently transmitted through LINC complex to the chromatin inside the nucleus, thereby resulting in increased telomere dynamics. Increased dynamics was also observed in the *LMNA* knockout experiment because the nucleus became devoid of its major structural element and could not maintain any spatial organization of the genome. This suggests a narrow window within which the chromatin organization can be maintained and regulated while filtering off high-frequency cytoskeletal fluctuations.

We also noted a slight increase in the fluctuation of telomere positions with respect to each other but no significant change in the rate of decay of their correlation (Fig. 4, *c* and *d*) upon overexpressing *LMNA* in the small circular condition.

Local fluctuations in telomere position are independent of cytoskeletal forces

The progressive increase in the α exponent with timescale (Fig. S3 *c*) means that telomere motion is highly constrained at small timescales and more directed at larger timescales. This could suggest that at small timescales, the telomeres move around a fixed central point, whereas at larger timescales, the central point itself moves. To investigate this further, we plotted the displacement of single telomeres as a function of time. A plot for a typical telomere from a rectangular cell and one from a circular cell is shown in Fig. 5 *a*. Though it is clearer in circular cells, in both conditions, we observed distinct displacement values around which the telomeres fluctuate for some time before moving to another position. To separate the motion of the center from the fluctuations around the center, the telomere trajectories were smoothed with a moving average filter to remove the high-frequency fluctuations. The smoothed positions will henceforth be referred to as the local mean positions. Fig. 5 *b* shows the trajectory of the local mean position superimposed on the corrected telomere trajectory for a typical telomere from a rectangular cell, as well as one from a circular cell. The residual from the moving average filter, which corresponds to the fluctuations of the telomeres around the tether, is shown in Fig. S7 *a*.

Confining cells to small circular substrates or subjecting them to a compressive load resulted in an increase in the speed with which the local mean positions moved (Fig. 5 *c*). No significant change was observed after TNF-α exposure (Fig. 5 *c*). Cytochalasin D and blebbistatin treatment on the large rectangular substrate caused an increase in the speed of the local mean position (Fig. 5 *d*), suggesting that the actomyosin stress fibers play a role in restricting the motion of the local mean position. Although blebbistatin treatment on the small circular condition resulted in a slight decrease in speed, it was not statistically significant.

Disruption of the nuclear lamina in $LMNA^{-/-}$ cells or nesprin 2G by DN-KASH transfection caused a marked increase in the speed with which the local mean positions moved. This, together with our earlier observations, points toward a model in which actin stress fibers from outside the nucleus are linked to telomeres inside the nucleus via transmembrane nesprin 2G, using the lamin A/C meshwork as a stable scaffold. Counterintuitively, overexpression of

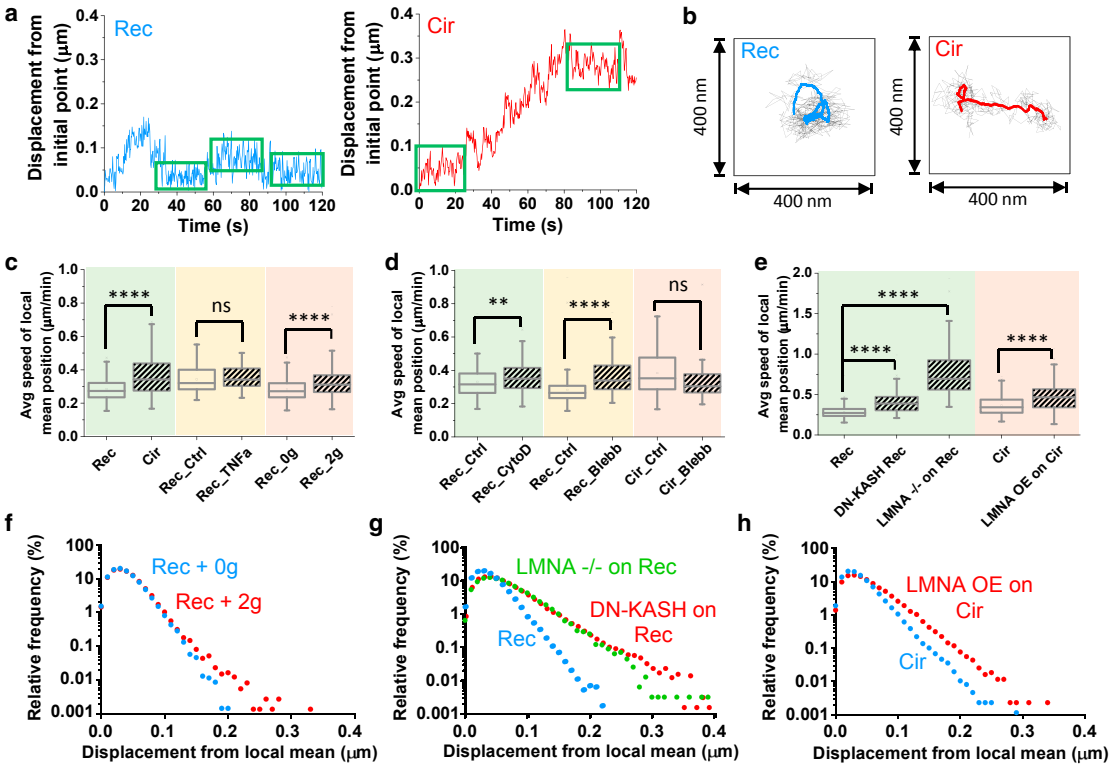

FIGURE 5 Cytoskeletal forces drive large-scale movement of telomeres while nucleoskeletal components regulate both the net movement and small-scale fluctuations. (*a*) Displacement versus time graphs for a single telomere from a rectangular cell (*left*) and one from a circular cell (*right*). (*b*) Corrected trajectories (*gray*) of a single telomere from a rectangular cell (*left*) and one from a circular cell (*right*), superimposed by the corresponding moving average filtered trajectories (*blue and red*). (*c–e*) The average speed of the smoothed telomere trajectories from populations of cells under the mentioned conditions. (*f–h*) Histograms of the residuals from the moving average filtered trajectories for populations of cells under the mentioned conditions. A Kolmogorov-Smirnov test was carried out to determine statistical significance.

lamin A/C in the small circular condition also resulted in an increase in the speed of the local mean position.

To analyze the fluctuations of the telomeres around their local means, we plotted the histograms of the residuals from the moving average filter. The histograms were plotted on a semilog scale to provide a zoomed-in view of the tails. We observed that neither cell shape nor TNF-α stimulation caused a marked change in fluctuations (Fig. S7 *b*). Interestingly, however, applying compressive load to the cells led to an increase in the displacements of the telomeres from their local mean positions (Fig. 5 *f*). Surprisingly, none of the drug treatment experiments (Fig. S7 *c*) recapitulated the increase that we observed with compressive load. This suggests that either the fluctuations of telomeres around their mean positions are regulated by events happening inside the nucleus or that compressive load acts via a pathway that is independent of the actomyosin contractility.

Even though actomyosin stress fibers did not have any effect on the fluctuation of telomeres around their local mean positions, overexpression of DN-KASH and knockout of lamin A/C resulted in an obvious intensification of the fluctuations in cells confined to rectangular substrates (Fig. 5 *g*). This means that the LINC complex and the nuclear lamina are important in keeping the telomeres close to their local mean positions. Based on this, we expected to see a decrease in the amplitude of fluctuations when we overexpressed lamin A/C in cells confined to circular patterns. Unexpectedly, we observed a further increase (Fig. 5 *h*).

TRF-1 binding dynamics at the telomeres is mechanically regulated

Single-molecule experiments have shown that altered tension on a DNA strand affects the ability of DNA binding proteins to bind to the strand (61). Therefore, after investigating how cytoskeletal dynamics and cytoskeletal interactions with the nucleoskeleton transduce extracellular stimuli into altered translational dynamics of telomeres, we were interested in understanding how the former impinges on the molecular and biological events occurring at the telomeres. To this end, we conducted FRAP experiments and examined the turnover of the telomere-binding protein TRF-1 at the telomeres (Fig. S8). Because of its DNA-binding domain, TRF-1 is a crucial component of the shelterin complex, which is located at all the telomeric regions of the genome throughout the cell cycle. This nucleoprotein complex decorates the entire telomeric chromatin and plays an important role in protecting telomere integrity. The

shelterin complex has also been shown to regulate transcription from the telomeres, which produces a noncoding RNA (TERRA) involved in maintaining the structure of telomeres.

Our FRAP results show an increase in the mobile fraction as well as recovery rate of TRF-1 upon depolymerization of actin stress fibers by CytoD (Fig. S8). This was also observed in cells confined to small circular substrates compared to the rectangular cells. Interestingly, overexpression of lamin A/C in the small circular cells restored the mobile fraction, as well as recovery rates, to values similar to those observed on the large rectangular condition. Given that overexpression of *LMNA* on the circular condition resulted in increased telomere dynamics, an increase in TRF-1 turnover was also expected. However, these results suggest that apart from altering telomere mobility, lamin A can also directly stabilize telomere-binding proteins onto the telomeres. This is in line with some recent publications on the interactions between *LMNA* and telomeric chromatin (62–64).

DISCUSSION

The composite structure formed by the cytoskeleton linking to the nuclear lamina and chromatin is an integral component to the regulation of genomic programs. Rather than being a static bridge that can only transmit forces, the cytoskeleton is a dynamic meshwork that can itself generate intracellular force fluctuations. Because these fluctuations are coupled to chromatin dynamics and regulated by the physical and chemical microenvironment of the cell, cytoskeletal dynamics provides an interface through which the cellular microenvironment influences chromatin dynamics. In line with this, we observed that in a well-spread cell, the nucleus is caged for a timescale of ~10 s (Fig. 1 *d*). This corresponds to the timescale at which Watanabe et al. observed large-scale actin depolymerization events in live fibroblasts (65). They also observed that the fastest depolymerization events start at timescales of ~4 s. Interestingly, this corresponds to the transition timescale we obtained for the nucleus when the extracellular conditions inhibited the formation of stable stress fibers (Fig. 1 *d*). Together, these findings suggest that the physical and chemical microenvironment can shift the proportion of actin turning over at different timescales, thereby altering the periodicity of force fluctuations experienced by the nucleus.

Chromatin is sensitive to the continuous fluctuation of forces generated by the cytoskeleton. We observed telomere translational dynamics within the nucleus to be tightly linked to the translational dynamics of the nucleus itself. These forces are not passively transmitted to the telomeres but rather are modulated by active mechanical bridges between the cytoskeleton and the telomeres. Depleting lamin A/C, for example, caused more than a 350% increase in the radius of constraint of telomeres, from ~75 to ~275 nm (Fig. 4 *a*). Instead of always being in subdiffusive territories, in the absence of lamin A/C, the telomeres transited into superdiffusive regimes within timescales of ~5 s. This observation is consistent with previous work in which telomere motion has been used as a proxy for studying chromatin dynamics (53).

Counterintuitively, increasing the levels of lamin A/C does not always lead to an increase in confinement of the telomeres. On small circular substrates, for instance, overexpression of *LMNA* led to an increase in the mean radius of constraint from 117 to 167 nm. This clearly demonstrates that neither the cytoskeleton nor the nucleoskeleton influences the telomeres in isolation, but rather, they function as a composite unit. When the cytoskeleton is stable, lamin A/C further confines telomere motion. When the cytoskeleton is dynamic, on the other hand, lamin A/C enhances telomere dynamics (Fig. 4 *a*), presumably by stiffening the lamina and allowing more efficient transmission of forces via nuclear membrane proteins to the chromatin.

Additionally, perinuclear "actin cap" or transmembrane actin-associated nuclear lines have been shown to regulate nuclear positioning and shape on similar microcontact systems (46,47). They will therefore likely contribute in regulating intranuclear dynamics as well. Because the formation of transmembrane actin-associated nuclear lines is dependent on *LMNA* levels and LINC complexes, further work in this direction might help us understand the molecular mechanism that would explain the counterintuitive results obtained by overexpressing lamin A in cells seeded on the small circular substrates.

Several studies have highlighted the interactions between telomeres and the nuclear lamina (62,63). These provide a means of mechanically coupling and allowing long-range interactions between loci that are distal in terms of genomic distances. Active force fluctuations imparted to the lamina from all around the nucleus thus result in correlated positional dynamics of spatially separated telomeres. Our results on telomere diffusion as well as correlated motion are in accordance with previous work in which the chromatin has been modeled as dense polymers, revealing microdomains of correlated dynamics by live imaging of fluorescently labeled H2B core histone (66,67). In this work, we show that these correlations, as well as the length scales over which they act, are strongly dependent on lamin A/C in the nuclear lamina (Fig. 4, *c* and *d*). Such chromatin dynamics could play an important role in genome mobilization observed upon DNA double-strand breaks, shown to be achieved by microtubule activity after telomere detachment from the nuclear membrane in budding yeast (28). In this context, it is noteworthy that earlier work revealed that nesprin 4 rather than 2 is involved in regulating telomere mobility upon telomeric damage in mouse embryonic fibroblasts (68). This suggests that cells have different pathways through which chromatin dynamics is regulated under

different cellular contexts. Our result is in line with observations that actin regulates chromatin dynamics under normal conditions in nonmigrating S-phase fibroblasts (38), whereas results reported in (68) are in line with observations that microtubules play the dominant role in regulating chromatin dynamics upon DNA damage. However, in an earlier study, we showed that there exists a cross-talk between the actin and microtubule networks in regulating nuclear morphology and chromatin dynamics (54).

Proper binding and unbinding dynamics of DNA binding proteins are critical for fine-tuning biological processes like transcription. In the case of telomeres, correct binding of TRF-1, an important component of the shelterin complex, has been shown to be essential for maintaining genomic integrity (7,8,10). Improper TRF-1 binding has been shown to result in genomic abnormalities similar to those observed in cancers. In this work, we demonstrated that increased cytoskeletal dynamics results in increased turnover of TRF-1 and further showed that overexpression of lamin A/C impedes the turnover (Fig. S8). This potentially provides a new angle to study telomeric instability in pathological contexts. Additionally, changes in the binding dynamics, as well as mobile fractions of TRF-1, could potentially provide a means of altering the exposure of telomeric sequences to other regulatory molecules or even damaging agents. In the control cells, which were confined to rectangular patterns, we recorded a mean TRF-1 mobile fraction of $\sim$0.1, which increased to $\sim$0.2 upon disruption of actin stress fibers. These values are higher compared to mobile fractions recorded for H2B core histones in cells on the same rectangular patterns, with ($\sim$0.11) and without ($\sim$0.075) disruption of F-actin (69). These results highlight the sensitivity of TRF-1 binding dynamics to cytoskeletal forces as well as nucleoskeletal stability.

Collectively, our results describe an important layer of regulation of telomere dynamics that is mediated by the intrinsic cytoskeletal fluctuations in addition to biochemical pathways. This mechanical regulation of telomere exposure by microenvironmental cues could therefore be an important aspect in the maintenance of telomere integrity. Given that the stability of the cytoskeleton is intimately linked to that of the lamina (and vice versa), our study highlights the importance of understanding telomere dynamics in the context of laminopathies, cytoskeleton-related diseases, and cancers.

SUPPORTING MATERIAL

Eight figures, two tables and one video are available at http://www.biophysj.org/biophysj/supplemental/S0006-3495(18)30983-4.

AUTHOR CONTRIBUTIONS

D.S.J. and G.V.S. designed research. D.S.J. and Y.S. performed research. D.S.J. and G.V.S. analyzed data. D.S.J. and G.V.S. wrote the manuscript.

ACKNOWLEDGMENTS

We thank Amit Singh, Jean-Francois Rupprecht, Madan Rao, and Jacques Prost for useful discussions. We thank Steven Wolf for critical reading of the manuscript and Mallika Nagrajan for helping with *TRF-1* transfections. Lamin A/C knockout mouse embryonic fibroblasts and nesprin DN-KASH plasmid were kind gifts from the Colin Stewart and Brian Burke laboratories. *TRF-1*-dsRed plasmid was a kind gift from Yuval Garini, Bar Ilan University.

We thank the Mechanobiology Institute, National University of Singapore, Singapore and Ministry of Education Tier-3 Grant Program (grant number MOE2012-T3-1-001) for funding.

REFERENCES

1. Bernal, A., and L. Tusell. 2018. Telomeres: implications for cancer development. *Int. J. Mol. Sci.* 19:E294.
2. Nene, R. V., C. D. Putnam, …, R. D. Kolodner. 2018. Cdc73 suppresses genome instability by mediating telomere homeostasis. *PLoS Genet.* 14:e1007170.
3. Sandin, S., and D. Rhodes. 2014. Telomerase structure. *Curr. Opin. Struct. Biol.* 25:104–110.
4. de Lange, T. 2009. How telomeres solve the end-protection problem. *Science.* 326:948–952.
5. Blackburn, E. H. 2001. Switching and signaling at the telomere. *Cell.* 106:661–673.
6. van Steensel, B., A. Smogorzewska, and T. de Lange. 1998. TRF2 protects human telomeres from end-to-end fusions. *Cell.* 92:401–413.
7. Iwano, T., M. Tachibana, …, Y. Shinkai. 2004. Importance of TRF1 for functional telomere structure. *J. Biol. Chem.* 279:1442–1448.
8. Okamoto, K., T. Iwano, …, Y. Shinkai. 2008. Distinct roles of TRF1 in the regulation of telomere structure and lengthening. *J. Biol. Chem.* 283:23981–23988.
9. Doksani, Y., J. Y. Wu, …, X. Zhuang. 2013. Super-resolution fluorescence imaging of telomeres reveals TRF2-dependent T-loop formation. *Cell.* 155:345–356.
10. Wang, L., Z. Tu, …, W. Li. 2018. Dual roles of TRF1 in tethering telomeres to the nuclear envelope and protecting them from fusion during meiosis. *Cell Death Differ.* 25:1174–1188.
11. Aviv, A., and J. W. Shay. 2018. Reflections on telomere dynamics and ageing-related diseases in humans. *Philos. Trans. R. Soc. Lond. B Biol. Sci.* 373:20160436.
12. Haycock, P. C., S. Burgess, …, G. Davey Smith; Telomeres Mendelian Randomization Collaboration. 2017. Association between telomere length and risk of cancer and non-neoplastic diseases: a mendelian randomization study. *JAMA Oncol.* 3:636–651.
13. Scheller Madrid, A., L. Rode, …, S. E. Bojesen. 2016. Short telomere length and ischemic heart disease: observational and genetic studies in 290 022 individuals. *Clin. Chem.* 62:1140–1149.
14. Zhan, Y., I. K. Karlsson, …, S. Hägg. 2017. Exploring the causal pathway from telomere length to coronary heart disease: a network mendelian randomization study. *Circ. Res.* 121:214–219.
15. Codd, V., C. P. Nelson, …, N. J. Samani; CARDIoGRAM Consortium. 2013. Identification of seven loci affecting mean telomere length and their association with disease. *Nat. Genet.* 45:422–427, 427e1–e2.
16. Gonzalo, S., R. Kreienkamp, and P. Askjaer. 2017. Hutchinson-Gilford Progeria syndrome: a premature aging disease caused by LMNA gene mutations. *Ageing Res. Rev.* 33:18–29.
17. Saha, B., G. Zitnik, …, J. Oshima. 2013. DNA damage accumulation and TRF2 degradation in atypical Werner syndrome fibroblasts with LMNA mutations. *Front. Genet.* 4:129.
18. Walsh, K. M., V. Codd, …, J. L. Wiemels; ENGAGE Consortium Telomere Group. 2015. Longer genotypically-estimated leukocyte telomere

length is associated with increased adult glioma risk. *Oncotarget.* 6:42468–42477.

19. Iles, M. M., D. T. Bishop, …, J. H. Barrett. 2014. The effect on melanoma risk of genes previously associated with telomere length. *J. Natl. Cancer Inst.* 106:dju267.
20. Machiela, M. J., J. N. Hofmann, …, M. P. Purdue. 2017. Genetic variants related to longer telomere length are associated with increased risk of renal cell carcinoma. *Eur. Urol.* 72:747–754.
21. Tanaka, H., E. A. Phipps, …, B. S. Herbert. 2018. Altered expression of telomere-associated genes in leukocytes among BRCA1 and BRCA2 carriers. *Mol. Carcinog.* 57:567–575.
22. Gunes, C., A. I. Avila, and K. L. Rudolph. 2018. Telomeres in cancer. *Differentiation.* 99:41–50.
23. Beishline, K., O. Vladimirova, …, P. M. Lieberman. 2017. CTCF driven TERRA transcription facilitates completion of telomere DNA replication. *Nat. Commun.* 8:2114.
24. Westmoreland, J. W., M. J. Mihalevic, …, M. A. Resnick. 2018. The global role for Cdc13 and Yku70 in preventing telomere resection across the genome. *DNA Repair (Amst.).* 62:8–17.
25. Ahmed, W., and J. Lingner. 2018. Impact of oxidative stress on telomere biology. *Differentiation.* 99:21–27.
26. Margalef, P., P. Kotsantis, …, S. J. Boulton. 2018. Stabilization of reversed replication forks by telomerase drives telomere catastrophe. *Cell.* 172:439–453.e14.
27. Stewart, J. A., Y. Wang, …, P. L. Schuck. 2018. Emerging roles of CST in maintaining genome stability and human disease. *Front. Biosci. (Landmark Ed).* 23:1564–1586.
28. Lawrimore, J., T. M. Barry, …, K. Bloom. 2017. Microtubule dynamics drive enhanced chromatin motion and mobilize telomeres in response to DNA damage. *Mol. Biol. Cell.* 28:1701–1711.
29. Bronshtein, I., I. Kanter, …, Y. Garini. 2016. Exploring chromatin organization mechanisms through its dynamic properties. *Nucleus.* 7:27–33.
30. Shivashankar, G. V. 2011. Mechanosignaling to the cell nucleus and gene regulation. *Annu. Rev. Biophys.* 40:361–378.
31. Chen, C. S., J. L. Alonso, …, D. E. Ingber. 2003. Cell shape provides global control of focal adhesion assembly. *Biochem. Biophys. Res. Commun.* 307:355–361.
32. Zhu, X., and R. K. Assoian. 1995. Integrin-dependent activation of MAP kinase: a link to shape-dependent cell proliferation. *Mol. Biol. Cell.* 6:273–282.
33. Choquet, D., D. P. Felsenfeld, and M. P. Sheetz. 1997. Extracellular matrix rigidity causes strengthening of integrin-cytoskeleton linkages. *Cell.* 88:39–48.
34. Li, W., J. Fan, and D. T. Woodley. 2001. Nck/Dock: an adapter between cell surface receptors and the actin cytoskeleton. *Oncogene.* 20:6403–6417.
35. Pawson, T., and J. D. Scott. 1997. Signaling through scaffold, anchoring, and adaptor proteins. *Science.* 278:2075–2080.
36. Juliano, R. L. 2002. Signal transduction by cell adhesion receptors and the cytoskeleton: functions of integrins, cadherins, selectins, and immunoglobulin-superfamily members. *Annu. Rev. Pharmacol. Toxicol.* 42:283–323.
37. Li, Q., A. Kumar, …, G. V. Shivashankar. 2014. The regulation of dynamic mechanical coupling between actin cytoskeleton and nucleus by matrix geometry. *Biomaterials.* 35:961–969.
38. Makhija, E., D. S. Jokhun, and G. V. Shivashankar. 2016. Nuclear deformability and telomere dynamics are regulated by cell geometric constraints. *Proc. Natl. Acad. Sci. USA.* 113:E32–E40.
39. Radhakrishnan, A. V., D. S. Jokhun, …, G. V. Shivashankar. 2017. Nuclear positioning and its translational dynamics are regulated by cell geometry. *Biophys. J.* 112:1920–1928.
40. Wang, Y., M. Nagarajan, …, G. V. Shivashankar. 2017. Orientation and repositioning of chromosomes correlate with cell geometry-dependent gene expression. *Mol. Biol. Cell.* 28:1997–2009.
41. Jain, N., K. V. Iyer, …, G. V. Shivashankar. 2013. Cell geometric constraints induce modular gene-expression patterns via redistribution of HDAC3 regulated by actomyosin contractility. *Proc. Natl. Acad. Sci. USA.* 110:11349–11354.
42. Mitra, A., S. Venkatachalapathy, …, G. V. Shivashankar. 2017. Cell geometry dictates TNFα-induced genome response. *Proc. Natl. Acad. Sci. USA.* 114:E3882–E3891.
43. Papantonis, A., T. Kohro, …, P. R. Cook. 2012. TNFα signals through specialized factories where responsive coding and miRNA genes are transcribed. *EMBO J.* 31:4404–4414.
44. Saxton, M. J. 1994. Anomalous diffusion due to obstacles: a Monte Carlo study. *Biophys. J.* 66:394–401.
45. Bronstein, I., Y. Israel, …, Y. Garini. 2009. Transient anomalous diffusion of telomeres in the nucleus of mammalian cells. *Phys. Rev. Lett.* 103:018102.
46. Luxton, G. W., E. R. Gomes, …, G. G. Gundersen. 2011. TAN lines: a novel nuclear envelope structure involved in nuclear positioning. *Nucleus.* 2:173–181.
47. Kim, D. H., S. Cho, and D. Wirtz. 2014. Tight coupling between nucleus and cell migration through the perinuclear actin cap. *J. Cell Sci.* 127:2528–2541.
48. Wang, N., J. D. Tytell, and D. E. Ingber. 2009. Mechanotransduction at a distance: mechanically coupling the extracellular matrix with the nucleus. *Nat. Rev. Mol. Cell Biol.* 10:75–82.
49. Crisp, M., Q. Liu, …, D. Hodzic. 2006. Coupling of the nucleus and cytoplasm: role of the LINC complex. *J. Cell Biol.* 172:41–53.
50. Tapley, E. C., and D. A. Starr. 2013. Connecting the nucleus to the cytoskeleton by SUN-KASH bridges across the nuclear envelope. *Curr. Opin. Cell Biol.* 25:57–62.
51. Wilson, K. L., J. M. Berk, and R. A. Quinlan. 2010. The nuclear envelope at a glance. *J. Cell Sci.* 123:1973–1978.
52. Chambliss, A. B., S. B. Khatau, …, D. Wirtz. 2013. The LINC-anchored actin cap connects the extracellular milieu to the nucleus for ultrafast mechanotransduction. *Sci. Rep.* 3:1087.
53. Bronshtein, I., E. Kepten, …, Y. Garini. 2015. Loss of lamin A function increases chromatin dynamics in the nuclear interior. *Nat. Commun.* 6:8044.
54. Ramdas, N. M., and G. V. Shivashankar. 2015. Cytoskeletal control of nuclear morphology and chromatin organization. *J. Mol. Biol.* 427:695–706.
55. Osmanagic-Myers, S., T. Dechat, and R. Foisner. 2015. Lamins at the crossroads of mechanosignaling. *Genes Dev.* 29:225–237.
56. De Vos, W. H., F. Houben, …, J. L. Broers. 2011. Repetitive disruptions of the nuclear envelope invoke temporary loss of cellular compartmentalization in laminopathies. *Hum. Mol. Genet.* 20:4175–4186.
57. Lammerding, J., L. G. Fong, …, R. T. Lee. 2006. Lamins A and C but not lamin B1 regulate nuclear mechanics. *J. Biol. Chem.* 281:25768–25780.
58. Pajerowski, J. D., K. N. Dahl, …, D. E. Discher. 2007. Physical plasticity of the nucleus in stem cell differentiation. *Proc. Natl. Acad. Sci. USA.* 104:15619–15624.
59. Lombardi, M. L., D. E. Jaalouk, …, J. Lammerding. 2011. The interaction between nesprins and sun proteins at the nuclear envelope is critical for force transmission between the nucleus and cytoskeleton. *J. Biol. Chem.* 286:26743–26753.
60. Sullivan, T., D. Escalante-Alcalde, …, B. Burke. 1999. Loss of A-type lamin expression compromises nuclear envelope integrity leading to muscular dystrophy. *J. Cell Biol.* 147:913–920.
61. Biebricher, A. S., I. Heller, …, G. J. L. Wuite. 2015. The impact of DNA intercalators on DNA and DNA-processing enzymes elucidated through force-dependent binding kinetics. *Nat. Commun.* 6:7304.
62. Burla, R., M. Carcuro, …, I. Saggio. 2016. The telomeric protein AKTIP interacts with A- and B-type lamins and is involved in regulation of cellular senescence. *Open Biol.* 6:160103.

63. Burla, R., M. La Torre, and I. Saggio. 2016. Mammalian telomeres and their partnership with lamins. *Nucleus.* 7:187–202.

64. Wood, A. M., J. M. Rendtlew Danielsen, …, S. T. Kosak. 2014. TRF2 and lamin A/C interact to facilitate the functional organization of chromosome ends. *Nat. Commun.* 5:5467.

65. Watanabe, N., and T. J. Mitchison. 2002. Single-molecule speckle analysis of actin filament turnover in lamellipodia. *Science.* 295:1083–1086.

66. Zidovska, A., D. A. Weitz, and T. J. Mitchison. 2013. Micron-scale coherence in interphase chromatin dynamics. *Proc. Natl. Acad. Sci. USA.* 110:15555–15560.

67. Nozaki, T., R. Imai, …, K. Maeshima. 2017. Dynamic organization of chromatin domains revealed by super-resolution live-cell imaging. *Mol. Cell.* 67:282–293.e7.

68. Lottersberger, F., R. A. Karssemeijer, …, T. de Lange. 2015. 53BP1 and the LINC complex promote microtubule-dependent DSB mobility and DNA repair. *Cell.* 163:880–893.

69. Toh, K. C., N. M. Ramdas, and G. V. Shivashankar. 2015. Actin cytoskeleton differentially alters the dynamics of lamin A, HP1α and H2B core histone proteins to remodel chromatin condensation state in living cells. *Integr. Biol.* 7:1309–1317.